Journal of The Electrochemical Society, **159** (10) A1747-A1754 (2012)
0013-4651/2012/159(10)/A1747/8/$28.00 © The Electrochemical Society

Optimization of the Cathode Structure of Lithium-Air Batteries Based on a Two-Dimensional, Transient, Non-Isothermal Model

Xianglin Li and Amir Faghri[z]

Department of Mechanical Engineering, University of Connecticut Storrs, Connecticut 06269, USA

A two-dimensional, transient, and non-isothermal model was developed in this work to study the mass transfer properties of the Li-air battery. Special attentions have been paid to the cathode carbon electrode and the distributions of oxygen, lithium ion, lithium peroxide, and temperature in the carbon electrode have been calculated in the model. The effects of discharge current, electrode thickness, porosity distribution in the electrode, and cathode open ratio on the discharge capacity of the battery have been investigated. Modeling results showed that the discharge capacity of a Li-air battery was primarily determined by the oxygen supply. Most of the available pores deep in the electrode were not utilized because Li_2O_2 accumulated at the electrode/air interface and blocked the oxygen. It was also found that the utilization rate of the electrode was lower when the electrode was thick, the cathode open ratio was low, and the discharge current was high. A unique design of the carbon electrode with a non-uniform porosity distribution was proposed, and the discharge capacity of the battery was increased by more than 25% after implementing the new electrode.
© 2012 The Electrochemical Society. [DOI: 10.1149/2.043210jes] All rights reserved.

Manuscript submitted June 15, 2012; revised manuscript received June 20, 2012. Published August 29, 2012.

In theory, the Li-air battery has an exceptionally high specific energy. This is largely due to the high specific energy of lithium, 12 kWh kg^{-1}, and the inexhaustible supply of oxygen from the ambient.[1] Although Li-air batteries have a high specific energy, the instability/corrosion of the lithium metal as the anode material has caused safety and reliability issues since the first primary Li-air battery was invented by Lockheed in the 1970 s.[2] These safety hurdles became more severe in the rechargeable Li-air battery and consequently impeded its development. In the meantime, Li-ion battery technology improved quickly after its first release by Sony in 1991. The Li-ion battery is safer than the Li-air battery and has a higher voltage efficiency and energy density than Lead-acid, Nickel-Cadmium, and Nickel metal hydride batteries. In the past two decades, Li-ion batteries have been widely applied to portable electronic devices, electric vehicles (EVs), photovoltaic panels, wind farms, and power grids. However, the high energy density required from portable devices and the 300 mile driving ranges required from electric vehicles both impose mass limitation on the existing Li-ion batteries. Considering the current specific energy of Li-ion batteries, about 0.1 kWh kg^{-1} for transportation applications, the battery in an EV must weigh more than 500 kg to drive the vehicle for 300 miles.

In order to decrease the weight, the specific energy of EV batteries should be significantly increased. For these reasons, special attention has recently been given to Li-air batteries due to their exceptionally high specific energy. In general, there are four types of lithium-air batteries, categorized by the electrolyte: organic electrolyte, aqueous electrolyte, mixed organic and aqueous electrolyte, and solid state electrolyte.[1] Of these, the battery using organic electrolytes (Fig. 1) has attracted the most attention because it is rechargeable when a sufficiently high voltage is applied.

The first rechargeable Li-air battery that utilized organic electrolytes was developed by Abraham and Jiang at the EIC Lab in 1996.[3] The Li-air battery operated passively at room temperature with lithium metal as the anode material and oxygen from the ambient as the oxidant. The overall reactions that occur during charge and discharge of a lithium-air battery using organic electrolyte are:

$$2Li + O_2 \leftrightarrow Li_2O_2 \quad (3.10\,V)\,, \qquad [1]$$

and/or

$$4Li + O_2 \leftrightarrow 2Li_2O \quad (2.91\,V)\,. \qquad [2]$$

The two-electron process in Eq. 1 is the dominant oxygen reduction reaction (ORR) under normal operating conditions.[3] During the discharge of the battery, lithium metal releases electrons and dissolves in the organic electrolyte as lithium ions. The lithium ions transport within the organic electrolyte, traveling through the separator to the cathode electrode. The electrons go through the out circuit, producing electric energy, to the cathode. At the same time, oxygen transports from the atmosphere into the cathode electrode and reacts with lithium ions and electrons, coming from the anode, at the surface of catalysts and/or carbon. The main product of the ORR is expected to be Li_2O_2, although the active intermediates during the ORR may react with organic electrolytes and produce Li_2CO_3, LiOH, and Lithium alkyl carbonate.[4,5] The detailed electrochemical reactions are not the main concern in this study due to the complex oxygen electrochemistry and the disagreements of reaction mechanisms among researchers.[6] In this work, it is assumed that Eq. 1 is the only reaction in the electrode and that Li_2O_2 is the only product during the battery discharge. The Li_2O_2 generated in the ORR does not dissolve in the electrolyte and covers the surface of catalysts and/or carbon. During the charge of the battery, the Li_2O_2 electrochemically decomposes into lithium ions, electrons, and oxygen. The lithium ions transfer within the organic electrolyte to the anode and produces lithium metal after reacting with the electrons coming from the cathode.

Currently, the major technical challenges of Li-air batteries using organic electrolytes are the low round trip efficiency (typically less than 70%) and the low current density (in the order of 1 mA cm^{-2}) during charge and discharge. It is worth noting that the experimental study by Zhang et al.[7] indicated that the power capability of lithium-oxygen batteries was mainly determined by the cathode carbon electrode. The low round trip efficiency, mainly determined by the overpotentials of ORRs and oxygen evolution reactions (OERs), can be increased by synthesizing advanced catalysts for both ORRs and OERs.[8–10] In 2010, a record high round trip efficiency of 75% was achieved by Lu et al. using PtAu/C as catalysts.[11] The low current density of a Li-air battery is caused by the combined effects of low catalytic activity, low Li^+ conductivity, low diffusivity of oxygen, and coverage of catalytic

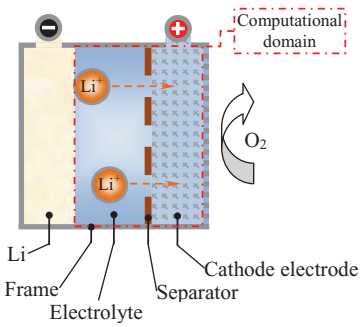

Figure 1. Computational domain of a lithium-air battery using organic electrolytes.

[z]E-mail: faghri@engr.uconn.edu

Downloaded on 2014-09-24 to IP 77.236.37.84 address. Redistribution subject to ECS terms of use (see ecsdl.org/site/terms_use) unless CC License in place (see abstract).

sites by solid products. Although the specific mechanism that limits the performance is still unclear, it is widely accepted that the mass transfer properties of the electrolyte and electrode play critical roles to determine the discharge current and capacity of a Li-air battery.[12]

Experimental studies have been carried out to investigate the electrolyte conductivity,[13] diffusivities of oxygen and lithium ion in electrolytes,[13,14] solubility of oxygen in organic electrolytes,[14] evaporation rate and water absorption rate of electrolytes,[15] and porosity and pore size distributions of the carbon electrode.[16–18] These experimental results are typically caused by combined changes of several parameters, as the parameters of the electrolyte and electrode are coupled with each other. The modeling studies of Li-air batteries can be a great help to understand the transport phenomena within the battery, study the effect of parameters, and improve the battery design. Nevertheless, only limited numbers of models have been developed to investigate the transport phenomena in Li-air batteries.

J. Read et al.[14] conducted a simple analysis to capture the dimensionless oxygen concentration along the carbon electrode depth after the steady-state condition was reached. The analysis was carried out with the assumptions that the discharge reaction was first order in the oxygen concentration only and that the porosity of the electrode did not change with Li_2O_2 production. Their results clearly showed that the oxygen concentration decreased with the increase of the depth to which oxygen penetrated the electrode. The decrease of oxygen was faster at a higher discharge current. Results also suggest that the increase of both oxygen solubility and diffusivity through the electrode and electrolyte would decrease the discharge overpotential.

Sandhu et al.[19] developed a one-dimensional, isothermal model to calculate the dimensionless oxygen concentration along the cathode carbon electrode. The variation of the pore radius over time due to the accumulation of Li_2O_2 solid was modeled at different discharge currents, and the effect of electrode thickness on the specific capacity was also calculated. Results showed that the specific capacity decreased with both the increase of discharge current and the increase of electrode thickness.

Zheng et al.[20] calculated the theoretical specific energy of Li-air batteries using different electrolytes: alkaline electrolytes, acidic electrolytes, and organic electrolytes. Their results showed that the battery with organic electrolytes had a higher specific energy and capacity than the battery with aqueous electrolytes because organic electrolyte was not consumed during the discharge. For example, when the porosity of cathode electrode was 0.7, the battery with organic electrolytes had a specific energy and capacity of 2.79 kWh kg^{-1} and 940 mAh g^{-1} respectively, while the battery with alkaline electrolytes had a specific energy and capacity of only 1.3 kWh kg^{-1} and 378 mAh g^{-1}.

Andrei et al.[21] developed a one-dimensional isothermal model to simulate oxygen and lithium ion concentrations and porosity distributions along the cathode carbon electrode. Based on this model, they proposed several approaches to optimize the structure of the cathode electrode: increasing the oxygen diffusivity and solubility; increasing the catalyst activity; using catalysts with non-uniform activity along the electrode; and applying partly wetted cathode electrode. The effects of the above parameters on specific capacity, energy density, and power density of the Li-air battery were studied by the model.

The mass transfer within a Li-air battery is dominated by two-dimensional effects. The commonly used nickel mesh in a passive battery as the supporting material[22,23] and the end plates with flow channels in active battery[24] inevitably block part of the oxygen path and decrease the cathode open ratio. However, none of the above models can capture the two-dimensional mass transfer characteristics of a Li-air battery. Modeling the non-uniform oxidant and production distributions in two dimensions are important to determine the battery performance. Furthermore, none of the above models consider the effect of temperature on the battery performance, though the thermal management of a Li-air battery plays a critical role in the safety and performance of batteries. In this work, we will develop a two-dimensional, transient, non-isothermal model to simulate the heat and mass transfer characteristics in the electrolyte and cathode air electrode of a Li-air battery using organic electrolytes.

Physical Model

This model uniquely considers the two-dimensional mass transfer and electrochemical reaction properties of the Li-air battery. The distributions of oxygen concentration, Li^+ concentration, reaction rate, and volume fraction of solid product will be solved in our model. The computational domain of the model includes the electrolyte and the cathode air electrode, as shown within the dashed line in Fig. 1.

To simplify the analysis and concentrate on the key parameters and phenomena, the following assumptions are adopted in this model:

1) The overpotential of the anode reaction is negligible.[7]
2) The electrolyte fully fills pores in the cathode electrolyte, both oxygen and lithium ion transfer in electrolyte (liquid) only.
3) The mass transfer of oxygen and lithium ion is by diffusion only, the effect of convection is negligible.
4) It is assumed that Li_2O_2 deposits as a smooth film in the electrode because the size of Li_2O_2 particles is typically several orders of magnitude smaller than the size of a Li-air battery electrode.[25]
5) Due to the high thermal conductivity of lithium metal, 84.8 W m^{-1} K^{-1}, and nickel mesh (which is commonly used as the supporting plate for the cathode electrode[7,22]), 90.9 W m^{-1} K^{-1}, their thermal resistances are negligible.

The concentration of lithium ion and dissolved oxygen are solved by:[26]

$$\frac{\partial\left(\varepsilon\rho_{\mathrm{EL}}\omega_{\mathrm{Li}^+}\right)}{\partial t}=\nabla\cdot\left(\rho_{\mathrm{EL}}D^{\mathrm{eff}}_{\mathrm{Li}^+}\nabla\omega_{\mathrm{Li}^+}\right)+\dot{m}_{\mathrm{Li}^+}, \quad [3]$$

and

$$\frac{\partial\left(\varepsilon\rho_{\mathrm{EL}}\omega_{\mathrm{O}_2}\right)}{\partial t}=\nabla\cdot\left(\rho_{\mathrm{EL}}D^{\mathrm{eff}}_{\mathrm{O}_2}\nabla\omega_{\mathrm{O}_2}\right)+\dot{m}_{\mathrm{O}_2}. \quad [4]$$

The effective diffusivity, D_i^{eff}, is determined by the diffusion coefficients, D_i, porosity of the porous media, ε, and tortuosity of the porous media, τ:

$$D^{\mathrm{eff}}_{i,g}=D_{i,g}\varepsilon^{\tau}, \quad [5]$$

where the tortuosity is a function of porosity:[27]

$$\tau(\varepsilon)=1-0.77\ln\varepsilon. \quad [6]$$

The consumption (/generation) rate in species equations of Li^+, and O_2 is:

$$\dot{m}_{\mathrm{Li}^+}=-\frac{R_{\mathrm{ORR}}}{F}M_{\mathrm{Li}}\quad\left[\frac{g}{m^3\cdot s}\right], \quad [7]$$

$$\dot{m}_{\mathrm{O}_2}=-\frac{R_{\mathrm{ORR}}}{2F}M_{\mathrm{O}_2}\quad\left[\frac{g}{m^3\cdot s}\right] \quad [8]$$

Where R_{ORR} is the reaction rate of the ORR, F is the Faradic constant, 96,487 C mol^{-1}, and M is the molecular weight.

The temperature distributions are calculated by solving the energy equation:[26]

$$\frac{\partial\left([\rho C_P]^{\mathrm{eff}}T\right)}{\partial t}=\nabla\cdot\left(\kappa_{\mathrm{T}}^{\mathrm{eff}}\nabla T\right)+\dot{m}_{\mathrm{T}}, \quad [9]$$

where the effective specific heat, $[\rho C_P]^{\mathrm{eff}}$, and the effective thermal conductivity, $\kappa_{\mathrm{T}}^{\mathrm{eff}}$, are related to the properties of electrode, Li_2O_2 precipitate, and electrolyte:

$$[\rho C_P]^{\mathrm{eff}}=(1-\varepsilon)\rho_{\mathrm{ED}}C_{P,\mathrm{ED}}+\varepsilon_{\mathrm{Li_2O_2}}\rho_{\mathrm{Li_2O_2}}C_{P,\mathrm{Li_2O_2}}+\left(\varepsilon-\varepsilon_{\mathrm{Li_2O_2}}\right)\rho_{\mathrm{EL}}C_{P,\mathrm{EL}}. \quad [10]$$

$$\kappa_T^{\mathrm{eff}}=(1-\varepsilon)\kappa_{\mathrm{ED}}+\varepsilon_{\mathrm{Li_2O_2}}\kappa_{\mathrm{Li_2O_2}}+\left(\varepsilon-\varepsilon_{\mathrm{Li_2O_2}}\right)\kappa_{\mathrm{EL}}. \quad [11]$$

Downloaded on 2014-09-24 to IP 77.236.37.84 address. Redistribution subject to ECS terms of use (see ecsdl.org/site/terms_use) unless CC License in place (see abstract).

The source terms used in the energy equations are also related to the electrochemical reaction:

$$\dot{m}_T = R_{ORR} \cdot \eta \quad \left[\frac{W}{m^3}\right], \qquad [12]$$

where η is the overpotential of the reaction.

The local ORR rate of the lithium-air battery is related to the concentrations of lithium ion and oxygen, the ORR coefficient, k_{ORR}, the surface area of the electrode per volume, A_{ED}, temperature, T, and the overpotential, η, by the following equation:

$$R_{ORR} = \left(\frac{\omega_{Li^+}}{\omega^{ref}_{Li^+}}\right) \cdot \left(\frac{\omega_{O_2}}{\omega^{ref}_{O_2}}\right) \cdot k_{ORR} \cdot A_{ED} \cdot \exp\left(\frac{\alpha_{ORR} F}{RT}\eta\right). \qquad [13]$$

The ORR coefficient, k_{ORR}, in the above reaction is a function of temperature:

$$k_{ORR} = i_0 \cdot \exp\left[\frac{E_{ORR}}{R}\left(\frac{1}{295} - \frac{1}{T}\right)\right], \qquad [14]$$

where i_0 is the exchange current density at 295 K, and E_{ORR} is the activation energy of the ORR, which has the value of 21 kJ mol^{-1} as an approximation.[28]

Since the produced Li_2O_2 is both insulating and insoluble in the electrolyte, the solid product deposits on the carbon surface and cause electrode surface passivation. The mechanism of electrode surface passivation is not fully understood because defects and grain boundaries in the crystal could result in different electronic properties of the Li_2O_2 layer.[29] In this model, the effect of electrode surface passivation is considered by decreasing the ORR coefficient with the deposition of Li_2O_2, as shown in Eq. 15. At the beginning of discharge, the deposition of Li_2O_2 gradually decreases the ORR coefficient due to the decrease of the effective surface area of the electrode. After the deposition of a single monolayer of Li_2O_2, the ORR coefficient is considered unchanged. Aurbach et al.[30] predicted that the charge during the production of a single monolayer Li_2O_2 was about 400 μC cm^{-2}. Considering the volumetric surface area of SP carbon, 69.3 cm^2 g^{-1}, and the electrode pore volume, 1.89 cm^3 g^{-1},[10] the charge during the production of a single monolayer Li_2O_2 per unit volume of electrode was 14.67 mC cm^{-3}. As a result, the volume faction of a single monolayer Li_2O_2 in the electrode is calculated to be 1.63×10^{-6}. The effect of the volume fraction of Li_2O_2 precipitate, ε_{Li2O2}, on the ORR coefficient is considered by a segmental equation:

$$k_{ORR} = \begin{cases} i_0 \cdot \left(1 - 0.9\dfrac{\varepsilon_{Li2O2}}{1.63 \times 10^{-6}}\right) & \text{for } \varepsilon_{Li2O2} < 1.63 \times 10^{-6} \\ 0.1 i_0 & \text{for } \varepsilon_{Li2O2} \geq 1.63 \times 10^{-6} \end{cases}. \qquad [15]$$

The above equation indicates that when the volume fraction of Li_2O_2 is less than 1.63×10^{-6}, the production of Li_2O_2 sediment will gradually cover the effective surface area of the electrode. When the volume fraction of Li_2O_2 is higher than 1.63×10^{-6}, a further increase of Li_2O_2 will not reduce the kinetics of ORR and only affects the diffusion of dissolved oxygen and lithium ions. The effective active area of electrode per volume, A_{ED}, is calculated by the following equation:

$$\frac{A_{ED}(t)}{A_{ED,0}} = \frac{\pi\left[d_{avg} - 2\delta_{Li_2O_2}(t)\right]^2}{\pi d^2_{avg}} = \left(1 - \frac{\varepsilon_{Li_2O_2}(t)}{\varepsilon}\right)^{2/3}, \qquad [16]$$

where $A_{ED,0}$ is the effective active area of the electrode before discharge, d_{avg} is the average size of the pores in electrode (0.1 μm[10]) and δ_{Li2O2} is the thickness of the Li_2O_2 precipitate.

The Li_2O_2 production rate from the ORR is calculated by:

$$\dot{m}_{Li_2O_2} = \frac{R_{ORR}}{2F} M_{Li_2O_2} \quad \left[\frac{g}{m^3 \cdot s}\right], \qquad [17]$$

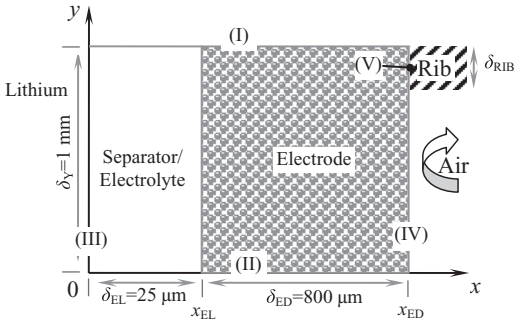

Figure 2. Boundary conditions of a lithium-air battery using organic electrolytes.

and the local volume fraction of Li_2O_2, ε_{Li2O2}, is calculated based on the amount of accumulated Li_2O_2:

$$\varepsilon_{Li_2O_2}(t) = \frac{\int R_{ORR} \cdot dt}{2F} \frac{M_{Li_2O_2}}{\rho_{Li_2O_2}}. \qquad [18]$$

The integration of the ORR rates within the whole computational domain equals the discharge current:

$$I = \int_{Electrode} R_{ORR} dx dy. \qquad [19]$$

Boundaries for the computational domain are numbered in Fig. 2. The upper (I) and lower (II) boundaries are considered to be symmetric boundaries and the corresponding boundary conditions are:

$$\frac{\partial \Phi}{\partial y} = 0, \qquad [20]$$

where Φ can be T, ω_{Li^+}, and ω_{O_2}.

At the lithium/separator interface (boundary III), the flux of lithium ion is proportional to the discharge current density:

$$N_{Li^+} = \rho D^{eff}_{Li^+} \nabla \omega_{Li^+} = \frac{I}{F} M_{Li} \quad \left[\frac{kg}{m^2 \cdot s}\right]. \qquad [21]$$

The flux of oxygen at boundary III is 0. Since the thermal resistance of lithium metal is assumed negligible, the temperature at boundary III is set as the room temperature:

$$T = T_\infty. \qquad [22]$$

At the electrode/air interface (boundary IV), the flux of lithium ion is 0 and the oxygen concentration is set as the saturation value:

$$\omega_{O_2} = 1.23 \times 10^{-4}. \qquad [23]$$

The heat flux through boundary IV is:

$$-\kappa^{eff}_T \frac{\partial T}{\partial x} = h(T - T_\infty). \qquad [24]$$

where the heat coefficient, h, is the natural convection coefficient on a vertical surface:[31]

$$Nu = \frac{hL}{k} = 0.68 + \frac{0.670 Ra_L^{1/4}}{\left[1 + (0.429/Pr)^{9/16}\right]^{4/9}}$$

$$\text{where } Ra_L = \frac{g\beta\Delta T L^3}{\alpha\nu}. \qquad [25]$$

At the electrode/rib interface (boundary V), the flux of lithium ion and oxygen are 0 and the temperature at boundary V is room temperature.

The computational grids were generated based on the finite volume method (FVM)[32] and the governing equations were discretized and solved by a code developed in home using Fortran. The grid number is 160 × 50 and the time step is 1 second. All the model results are both grid independent and the time step independent. After the results

Downloaded on 2014-09-24 to IP 77.236.37.84 address. Redistribution subject to ECS terms of use (see ecsdl.org/site/terms_use) unless CC License in place (see abstract).

Table I. Parameters used in the model.

Parameter	Symbol	Value
Room temperature	T_∞	297 K
Thermal diffusivity of air	α	2.22×10^{-5} m^2 s^{-1}
Kinematic viscosity of air	ν	1.51×10^{-5} m^2 s^{-1}
Thermal expansion coefficient of air	β	3.43×10^{-3} K^{-1}
Prandtl number of air	Pr	0.713
Active area of electrode per volume	$A_{ED,0}$	3.67×10^5 cm^2 cm^{-3} 10
Exchange current density	i_0	3.11×10^{-4} A cm^{-2} 33
Transfer coefficient of cathode	α_{ORR}	0.5 33
Thermodynamic equilibrium voltage	E_0	3. 1 3
Reference concentration of O_2	$\omega_{O_2}^{ref}$	1.23×10^{-4} kg kg^{-1}
Reference concentration of lithium ion	$\omega_{Li^+}^{ref}$	6.67×10^{-3} kg kg^{-1}
Density of PTFE	ρ_{PTFE}	2.2 g cm^{-3}
Density of lithium	ρ_{Li}	0.534 g cm^{-3}
Density of carbon	ρ_C	2.26 g cm^{-3}
Density of lithium peroxide	ρ_{Li2O2}	2.31 g cm^{-3}
Density of electrolyte	ρ_{EL}	1.0402 g cm^{-3} 15
Conductivity of electrolyte	σ_{EL}	5×10^{-3} Ω^{-1} cm^{-1} 15
Conductivity of electrode	σ_{ED}	3 Ω^{-1} cm^{-1} 34
Specific heat of electrolyte	$C_{P,EL}$	0.5 J g^{-1} K^{-1}
Specific heat of carbon	$C_{P,ED}$	0.71 J g^{-1} K^{-1}
Specific heat of Li_2O_2	$C_{P,Li2O2}$	1.81 J g^{-1} K^{-1}
Diffusivity of oxygen in electrolyte	D_{O2}	1×10^{-5} cm^2 s^{-1} 34
Diffusivity of Li^+ in electrolyte	D_{Li+}	8×10^{-7} cm^2 s^{-1} 34
Thermal conductivity of electrolyte	k_{EL}	0.2 W m^{-1} K^{-1}
Thermal conductivity of electrode	k_{ED}	1.5 W m^{-1} K^{-1} 35
Thermal conductivity of Li_2O_2	k_{Li2O2}	14.5 W m^{-1} K^{-1}
Solubility of oxygen in electrolyte		4×10^{-3} M 14
Molecular weight of lithium	M_{Li}	6.94 g mol^{-1}
Molecular weight of lithium peroxide	M_{Li2O2}	45.88 g mol^{-1}
Porosity of electrode	ε_{ED}	0.75 10
Porosity of separator	ε_{EL}	0.5 10
Thickness of the electrode	δ_{ED}	800 μm 22
Thickness of the separator	δ_{EL}	25 μm 10
Width of the battery	δ_Y	1 mm
Width of the rib	δ_{RIB}	0 ~ 0.5 mm

are converged in each time step, the cell voltage is determined by the following equation:

$$V = E_0 - \eta - I \times (\delta_{EL}/\sigma_{EL}), \quad [26]$$

where E_0 is the thermodynamic equilibrium voltage, δ_{EL} is the thickness of the separator, and σ_{EL} is the conductivity of the electrolyte. Values of parameters used in the model are all presented in Table I.

Results

Comparison of modeling results with experimental data.— After the grid and time-independent verification of our model, the discharge capacity vs. voltage at various discharge current densities (0.05, 0.1, 0.2, 0.5 mA cm^{-2}) were calculated and compared with the experimental data reported by Read[22] in Fig. 3. At the beginning of discharge, the battery voltage rapidly decreases from the ideal voltage as a result of the activation loss caused by the ORR. Afterwards, a voltage plateau is observed, followed by a quick decrease in voltage at the end of the discharge caused by the concentration loss due to limited mass transfer rates.

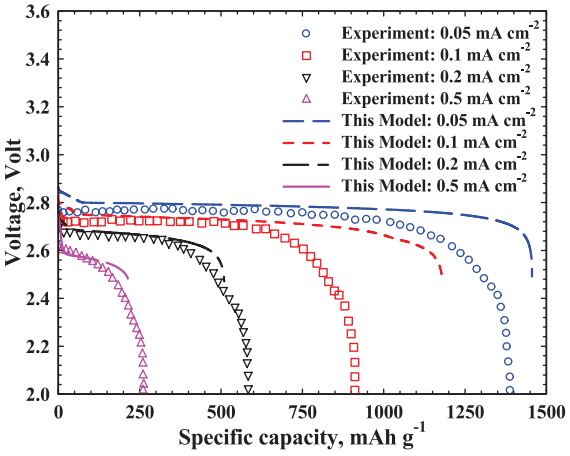

Figure 3. Comparisons between modeling results and experimental data[22] of specific capacities vs. voltage at different discharge current densities.

Similar to the reported experimental data, our simulation results showed that the voltage of the battery was higher at a smaller discharge current for a given specific capacity. For example, at the specific capacity of 200 mAh g^{-1}, the voltage was 2.85, 2.79, 2.74, and 2.63 V at the discharge current of 0.05, 0.1, 0.2, and 0.5 mA cm^{-2}, respectively. The decrease in voltage was due to the higher overpotentials caused by activation loss, ohmic resistance and concentration loss at a higher discharge current. Since the organic electrolyte has relatively low ionic conductivity and low oxygen and lithium ion diffusivities, the overpotential caused by ohmic loss and concentration loss is significant even at small discharge currents.

The simulation results in Fig. 3 also showed that the maximum specific capacity of the battery was higher at a smaller discharge current, which was consistent with experimental results.[22] The maximum specific capacity decreased from 1454 to 1180, 535, and 214 mAh g^{-1} when the discharge current density increased from 0.05 to 0.1, 0.2, and 0.5 mA cm^{-2}. The volume fractions of Li_2O_2 after discharging were plotted in Fig. 4. The non-dimensional x in this figure and the

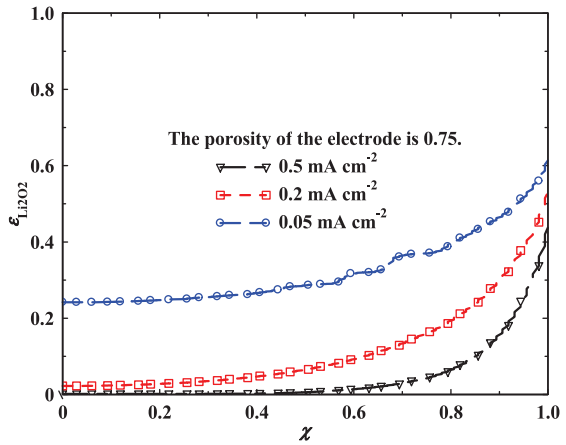

Figure 4. Volume fractions of Li_2O_2 in the electrode after the battery discharged at various current densities.

Downloaded on 2014-09-24 to IP 77.236.37.84 address. Redistribution subject to ECS terms of use (see ecsdl.org/site/terms_use) unless CC License in place (see abstract).

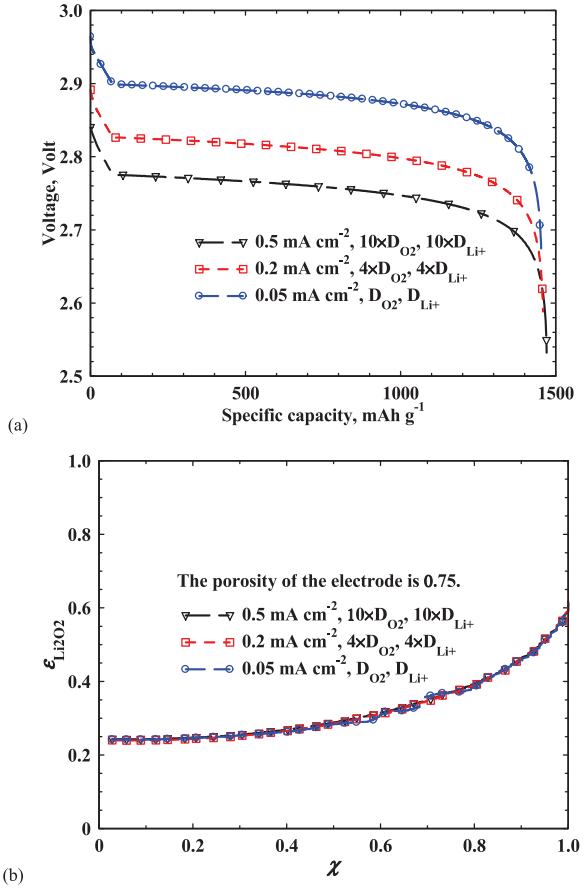

Figure 5. (a) Specific capacities vs. voltage and (b) volume fractions of Li_2O_2 in the electrode at different discharge current densities. Diffusivities of lithium ion and oxygen are adjusted according to the current density.

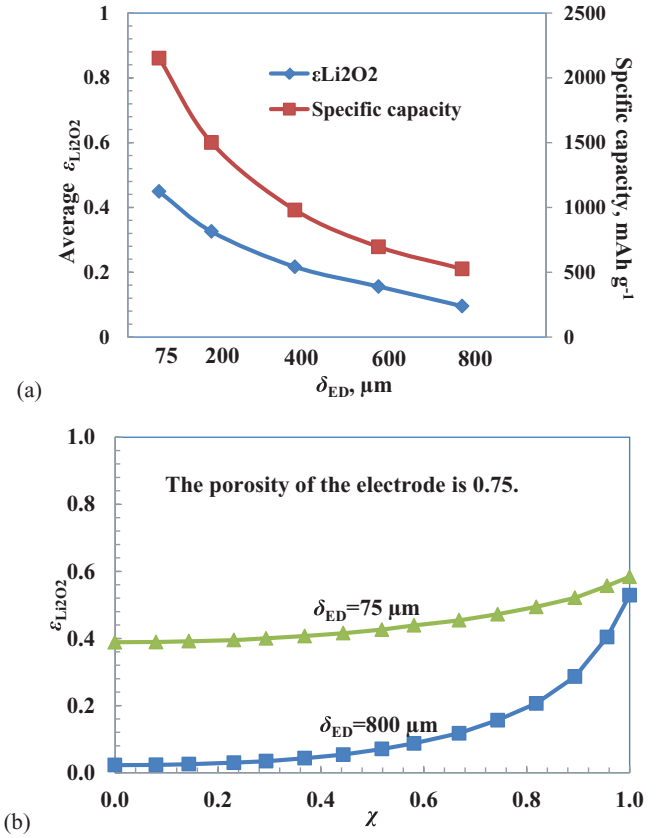

Figure 6. (a) Specific capacities and average volume fractions of Li_2O_2 vs. electrode thickness at a 0.2 mA cm^{-2} discharging rate, (b) volume fractions of Li_2O_2 in electrodes with different thicknesses.

following figures is defined as:

$$\chi = (x - \delta_{EL})/\delta_{ED}. \quad [27]$$

At the electrode/air interface, the variation of volume fractions of Li_2O_2 was small: 0.61, 0.53, and 0.44 at the current density of 0.05, 0.2, and 0.5 mA cm^{-2}, respectively. The volume fraction of Li_2O_2 at the separator/electrode interface, however, decreased sharply from 0.24 to 0.02 and 0.002 when the current density increased from 0.05 to 0.2 and 0.5 mA cm^{-2}. This result indicated that most pores close to the separator were not utilized because of the insufficient oxygen supply, and the non-uniform utilization of the electrode was more severe at higher current densities.

Model results show that the maximum temperature rise in the battery is less than 0.01 K at the highest current density (0.5 mA cm^{-2}). The low temperature increase in the battery is due to the low heat generation rate and the effective cooling by natural convection. The heat generation rate in the battery is low because the discharge current density is small. Furthermore, the battery has a high ratio of surface area to volume, so that the produced heat is effectively dissipated to the ambient by natural convection. Consequently, the results of temperature distributions will not be shown in this work.

Effect of the diffusivities of oxygen and lithium ion.— Considering this, the diffusivities of oxygen and lithium ion were adjusted according to the discharge current in the model in order to study its effect on the discharge capacity. Fig. 5a shows the specific capacities vs. voltage curves at various discharge current densities. Taking 0.05 mA cm^{-2} as the base case, diffusivities of oxygen and lithium were multiplied by 4 and 10 at 0.2 and 0.5 mA cm^{-2}, respectively. Although the voltage at a given specific capacity was lower at a higher current density due to the higher ohmic loss, the maximum specific capacities were identical for all the three cases. The volume fractions of Li_2O_2 depicted in Fig. 5b showed that by increasing the diffusivities of oxygen and lithium ion, the maximum specific capacity increased, mainly due to the more efficient utilization of the electrode close to the separator. It can be concluded from these results that the mass transfer limitation, especially oxygen transfer, was decisive to the maximum discharge capacity of a Li-air battery.

Effect of the electrode thickness.— As is discussed above, the specific capacity is determined by mass transfer limitation, so the electrode thickness is an important design parameter to achieve high specific capacity. Fig. 6a compares the specific capacity vs. voltage curves of batteries with different electrode thicknesses, where all the batteries were discharged at 0.2 mA cm^{-2}. As can be seen from the figure, the specific capacity was 2151, 1500, 980, 696, and 526 mAh g^{-1} when the electrode thickness was 75, 200, 400, 600, and 800 μm, respectively. The average volume fractions of Li_2O_2 after discharge were also compared in Fig. 6a, and a lower specific capacity corresponded with a lower average volume fraction of Li_2O_2. These results also showed that the battery with a thicker electrode had a lower utilization rate of its electrode. The volume fraction of Li_2O_2 was only 9.5% when the electrode thickness was 800 μm, although the capacity limit was to fill 75% (porosity) of the electrode with Li_2O_2. This conclusion was consistent with the experimental investigations. For example, studies by Ren et al.[10] showed that only 10% of the pore volume was covered by Li_2O_2, even when the discharge capacity was as high as 1,000 mAh g^{-1}.

The volume fractions of Li_2O_2 along the electrodes are plotted in Fig. 6b. The results clearly showed that the accumulation of Li_2O_2 was faster close to the air side, and the non-uniform Li_2O_2 distribution

Downloaded on 2014-09-24 to IP 77.236.37.84 address. Redistribution subject to ECS terms of use (see ecsdl.org/site/terms_use) unless CC License in place (see abstract).

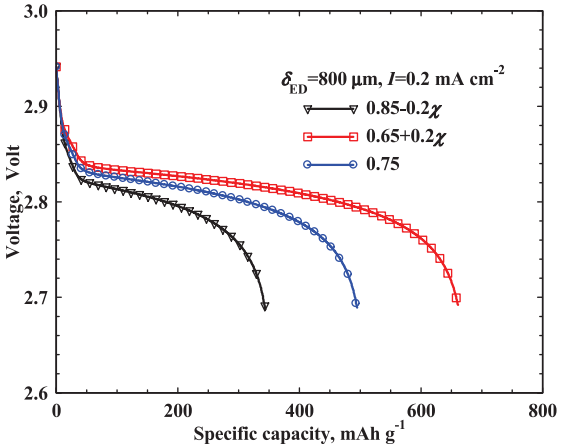

Figure 7. Voltage vs. specific capacities curves of electrodes with different porosity distributions: blue circle - uniform porosity; red rectangle - high porosity at the air side; black triangle - lower porosity at the air side.

was more severe when the electrode was thicker. Due to the limited oxygen diffusivities, the reaction rates in the electrode were non-uniform, with higher reaction rates close to the electrode/air interface and lower reaction rates close to the electrode/separator interface. For the battery with a thick electrode (800 μm), most of the electrode was not fully used due to the blockage of oxygen by the faster Li_2O_2 accumulation at the electrode/air interface. To make better use of all the pores throughout the electrode, it is preferable to design a Li-air battery with a thinner electrode.

The effect of porosity distribution.— From the previous discussion, it is known that most of the pores in the cathode electrode are not utilized during the battery discharge. This phenomenon is due to the lack of oxygen. To improve the battery design, it is critical to improve the mass transfer properties of the electrode. One important parameter of the electrode that can be easily changed is the porosity distribution. In our model, the average porosity of the electrode was kept constant, 0.75. Three porosity distributions have been studied: uniform distribution, linear distribution with a high porosity at the air side, and linear distribution with a lower porosity at the air side. Fig. 7 shows the specific capacity vs. voltage curves of electrodes with 800 μm and various porosity distributions where all batteries are discharged at 0.2 mA cm^{-2}. As shown in Fig. 7, the electrode with a higher porosity at the air side had the highest specific capacity, 661 mAh g^{-1}, while the electrode with a lower porosity at the air side had the lowest specific capacity, 495 mAh g^{-1}.

The different specific capacities of batteries were caused by the different utilization rates of these three electrodes, despite the fact that they had the same average porosity, 0.75. The distributions of porosity and volume fractions of Li_2O_2 after discharge are compared in Fig. 8. As shown in Fig. 8, the volume fractions of Li_2O_2 were non-uniform within the electrode for both electrodes. However, the electrode with a higher porosity at the air side had a better utilization of pores deep in the electrode due to the more efficient oxygen transfer from the ambient. The effective porosity, shown in the Fig. 8, equals the local porosity minus the volume fraction of Li_2O_2. The effective porosity close to the air side is more important, however, because all of the consumed oxygen should be supplied from the air side. During the discharge, Li_2O_2 was produced faster close to the air side because of the non-uniform oxygen distribution. As a result, the effective porosity decreased faster close to the air side. Eventually, the oxygen supply rate was so low that the oxygen concentration close to the separator was near zero and the battery therefore stopped discharging. When the porosity at the air side was higher, the oxygen supply was more sufficient throughout the electrode and the discharging of battery lasted longer. Consequently, local volume fractions of Li_2O_2 were higher throughout the electrode with a higher porosity at the

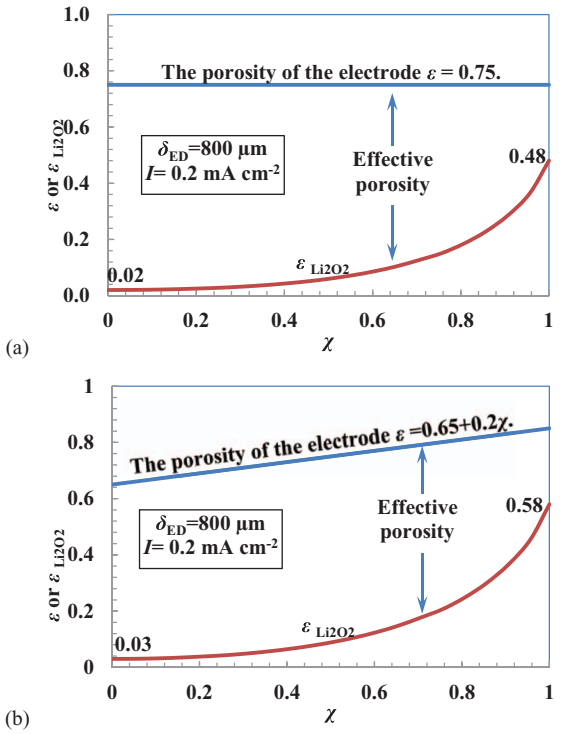

Figure 8. Distributions of porosity and Li_2O_2 volume fraction in the electrode after discharge: (a) uniform porosity distribution, and (b) a higher porosity at the air side.

air side. It should be recognized that the total amount of produced Li_2O_2 is proportional to the specific discharge capacity of the battery. This study shows that it is possible to increase the battery discharge capacity by more than 25% after increasing the electrode porosity at the air side.

The effect of cathode open ratios.— All the above modeling results were achieved with the assumption of 100% cathode open ratio, however, the 100% open ratio at the cathode side is not procurable in either passive or active Li-air battery designs. The nickel mesh and the end plates inevitably block part of the oxygen pathway or decrease the cathode open ratio.[22–24] Considering this, the specific capacity vs. voltage curves with different cathode open ratios were calculated and plotted in Fig. 9, and all of the batteries are discharged at 0.2 mA cm^{-2}. As expected, both the battery voltage and the discharge

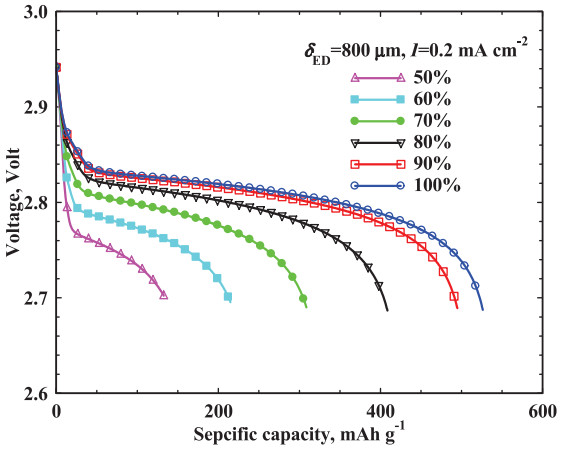

Figure 9. Voltage vs. specific capacities of batteries with different cathode open ratios.

Downloaded on 2014-09-24 to IP 77.236.37.84 address. Redistribution subject to ECS terms of use (see ecsdl.org/site/terms_use) unless CC License in place (see abstract).

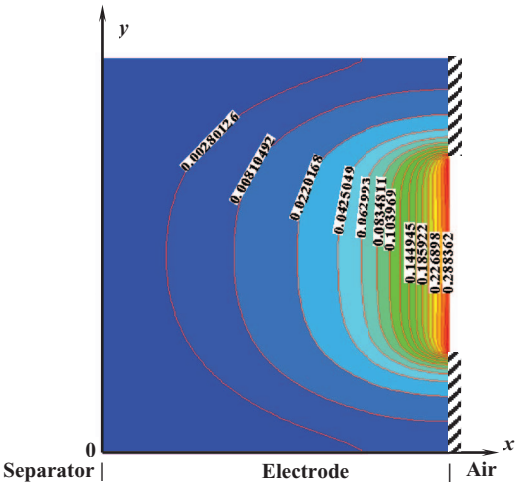

Figure 10. Volume fractions of Li_2O_2 in the electrode with 50% open ratio after discharging, the electrode has an 800 μm thickness and is discharged at 0.2 mA cm^{-2}.

capacity decreased with a decreasing open ratio due to the limitation of oxygen supply. The maximum capacities sharply decreased (from 529 to 133) when the cathode open ratio decreased from 100% to 50%.

The Li_2O_2 volume fraction in electrodes with a 50% open ratio is plotted in Fig. 10. As shown in the figure, the Li_2O_2 volume fractions at the electrode/air interfaces were the highest (0.29). Both the Li_2O_2 volume fractions close to the separator and under the rib, however, were extremely low. This result shows that the pores under the rib and deep in the electrode were both barely utilized. The Li_2O_2 volume fractions in these areas were less than 0.02. To design a Li-air battery, the open ratio of the cathode should be as high as possible, especially when the battery discharges at high currents. If the open ratio of the cathode with flow channels is low in an active battery design, the forced convection has to be involved to facilitate the mass transfer within the electrode.

Conclusions

The Li-air battery has exceptionally high specific energy due to the high specific energy of lithium and the inexhaustible oxygen supply from ambient. However, state-of-the-art studies on transport phenomena have yet to fully utilize the great potential of Li-air batteries. This is mainly a result of the mass transfer limitation of the cathode electrode. In this study, a two-dimensional, transient, and non-isothermal model has been developed to study the mass transfer properties of Li-air batteries. After investigating various parameters, such as discharge current, electrode thickness, porosity distribution in the electrode, and cathode open ratio of the battery, the following conclusions and recommendations have been proposed to improve the Li-air battery design:

1) Mass transfer properties of the carbon electrode determined the discharge current and capacity of a Li-air battery. During discharge, a Li-air battery starved from a lack of oxygen because the produced Li_2O_2 accumulated quickly over time at the electrode/air interface.
2) The discharge capacity of a Li-air battery could be remarkably increased by utilizing the pores deep in the carbon electrode more efficiently. For example, the volume fraction of Li_2O_2 in an 800-μm-thick electrode was less than 10% when the battery reached its maximum discharge capacity, at a current density of 0.2 mA cm^{-2}.
3) The maximum specific capacity of a Li-air battery could be increased by decreasing the thickness of the carbon electrode, increasing the porosity at the electrode/air interface, and increasing the cathode open ratio to facilitate oxygen transfer.
4) The maximum discharge capacity decreased from 2151 to 526 mAh g^{-1} when the electrode thickness increased from 75 to 800 μm. The maximum specific capacity decreased from 526 to 133 mAh g^{-1} by decreasing the open ratio from 100% to 50% at the current density of 0.2 mA cm^{-2}.
5) Keeping the average porosity constant, 0.75, the electrode with a higher porosity at the electrode/air interface had a higher specific capacity, 661 mAh g^{-1}, than that of the electrode with uniform porosity, 526 mAh g^{-1}.

List of Symbols

A_{ED}	the surface area of the electrode per volume (m^{-1})
C_p	specific heat capacity (J mol^{-1} K^{-1})
D	diffusivity (m^2 s^{-1})
E_0	thermodynamic equilibrium voltage (V)
E_{ORR}	activation energy of the ORR (kJ mol^{-1})
F	Faraday constant (96,487 C mol^{-1})
Ra	Rayleigh number
h	natural convection coefficient (W m^{-1} K^{-1})
I	current density (A m^{-2})
i_0	exchange current density (A m^{-3})
K	permeability (m^2)
k_{ORR}	oxygen reduction reaction coefficient
M	molecular weight (kg mol^{-1})
$\dot{m}$	mass consumption or generation rate (g m^{-3} s^{-1})
$\dot{m}_T$	heat consumption or generation rate (W m^{-3})
N_{Li+}	flux of lithium ion (kg s^{-1} m^{-2})
Pr	Prandtl number
R	ideal gas constant (8.314 J mol^{-1} K^{-1})
R_{ORR}	reaction rate of oxygen reduction reaction (A m^{-3})
T	cell temperature (°C)
V	voltage (V)

Greek

α	thermal diffusivity
α_{ORR}	transfer coefficient of ORR
δ	thickness
ε	porosity
ε_{Li2O2}	volume fraction of Li_2O_2
η	over potential (V)
k	thermal conductivity (W K^{-1} m^{-1})
μ	dynamic viscosity (kg m^{-1} s^{-1})
ν	kinematic viscosity (m^2 s^{-1})
ρ	density (kg m^{-3})
σ	surface tension (N m^{-1})
σ_m	conductivity of Nafion (Ω^{-1} m^{-1})
τ	tortuosity
χ	Non-dimensional x
ω	mass fraction (kg kg^{-1})

Superscripts and Subscripts

0	initial value
avg	average value
ED	electrode
EL	electrolyte
eff	effective value in porous layer
i	species i
ORR	oxygen reduction reaction
ref	reference value

Acronyms

EV	Electric vehicle
FVM	Finite volume method
OER	Oxygen evolution reactions
ORR	Oxygen reduction reaction

Downloaded on 2014-09-24 to IP 77.236.37.84 address. Redistribution subject to ECS terms of use (see ecsdl.org/site/terms_use) unless CC License in place (see abstract).

References

1. G. Girishkumar, B. McCloskey, A. C. Luntz, S. Swanson, and W. Wilcke, *J. Physical Chemistry Letters*, **1**, 2193 (2010).
2. W. R. Momyer and E. L. Littauer, Development of a lithium-water-air primary battery. *Proceedings of the Intersociety Energy Conversion Engineering Conference*, **2**, 1480 (1980).
3. K. M. Abraham and Z. Jiang, *J. Electrochem. Soc.*, **143**, 1 (1996).
4. S. A. Freunberger, Y. Chen, N. E. Drewett, L. J. Hardwick, F Bardé, and P. G. Bruce, *Angewandte Chemie - International Edition*, **50**, 8609 (2011).
5. S. A. Freunberger, Y. Chen, Z. Peng, J. M. Griffin, L. J. Hardwick, F. Bardé, P. Novák, and P. G. Bruce, *Journal of the American Chemical Society*, **133**, 8040 (2011).
6. Y. Shao, S. Park, J. Xiao, J. G. Zhang, Y. Wang, and J. Liu, *ACS Catalysis*, **2**, 844 (2012).
7. S. S. Zhang, D. Foster, and J. Read, *J. Power Sources*, **195**, 1235 (2010).
8. A. Débart, J. Bao, G. Armstrong, and P. G. Bruce, *J. Power Sources*, **174**, 1177 (2007).
9. Y. C Lu, H. A. Gasteiger, M. C. Parent, V. Chiloyan, and Y. Shao-Horn, *Electrochemical and Solid-State Letters*, **13**, A69 (2010).
10. X. Ren, S. S. Zhang, D. T. Tran, and J. Read, *J. Materials Chemistry*, **21**, 10118 (2011).
11. Y. C. Lu, Z. Xu, H. A. Gasteiger, S. Chen, K. Hamad-Schifferli, and Y. Shao-Horn, *J. Am. Chem. Soc.*, **132**, 12170 (2010).
12. R. Padbury and X. Zhang, *J. Power Sources*, **196**, 4436 (2011).
13. D. Aurbach, Nonaqueous Electrochemistry: An Overview, *Nonaqueous Electrochemisty*, 1st ed., Marcel Dekker, Inc., New York, 1999, pp. 1–52.
14. J. Read, K. Mutolo, M. Ervin, W. Behl, J. Wolfenstine, A. Driedger, and D. Foster, *J. Electrochem. Soc.*, **150**, A1351 (2003).
15. W. Xu, J. Xiao, J. Zhang, D. Wang, and J. G. Zhang, *J. Electrochem. Soc.*, **156** A773 (2009).
16. X. H. Yang, P. He, and Y. Y. Xia, *Electrochemistry Communications*, **11**, 1127 (2009).
17. S. R. Younesi, S. Urbonaite, F. Björefors, and K. Edström, *J. Power Sources*, **196**, 9835 (2011).
18. C. Tran, X. Q. Yang, and D. Qu, *J. Power Sources*, **195**, 2057 (2010).
19. S. S. Sandhu, J. P. Fellner, and G. W. Brutchen, *J. Power Sources*, **164**, 365 (2007).
20. J. P. Zheng, R. Y. Liang, M. Hendrickson, and E. J. Plichta, *J. Electrochem. Soc.*, **155**, A432 (2008).
21. P. Andrei, J. P. Zheng, M. Hendrickson, and E. J. Plichta, *J. Electrochem. Soc.*, **157**, A1287 (2010).
22. J. Read, *J. Electrochem. Soc.*, **149**, A1190 (2002).
23. J. G. Zhang, D. Wang, W. Xu, J. Xiao, and R. E. Williford, *J. Power Sources*, **195**, 4332 (2010).
24. J. Adams and M. Karulkar, *J. Power Sources*, **199**, 247 (2012).
25. R. R. Mitchell, B. M. Gallant, C. V. Thompson, and Y. Shao-Horn, *Energy & Environmental Science*, **4**, 2952 (2011).
26. A. Faghri and Y. Zhang, *Transport Phenomena in Multiphase Systems*, Elsevier Inc., (2006).
27. M. Matyka, A. Khalili, and Z. Koza, *Physical Review E - Statistical, Nonlinear, and Soft Matter Physics*, **78**, 026306 (2008).
28. A. B. Anderson, J. Roques, S. Mukerjee, V. S. Murthi, N. M. Markovic, and V. Stamenkovic, *J. Phys. Chem. B.*, **109**, 1198 (2005).
29. J. Christensen, P. Albertus, R. S. Sanchez-Carrera, T. Lohmann, B. Kozinsky, R. Liedtke, J. Ahmed, and A. Kojic, *J. Electrochemical Society*, **159** R1 (2012).
30. D. Aurbach, M. Daroux, P. Faguy, and E. Yeager, *J. Electroanal. Chem.*, **297** 225 (1991).
31. T. L. Bergman, D. P. DeWitt, F. P. Incropera, and A. S. Lavine, *Fundamentals of Heat and Mass Transfer*, Wiley, John & Sons, Incorporated, (2011) 605.
32. S. V. Patankar, *Numerical Heat and Fluid Flow*, Hemisphere Publishing Corporation, (1980).
33. C. O'Laoire, Investigations of oxygen reduction reactions in non-aqueous electrolytes and the lithium-air battery, *Northeastern University Dissertation*, (2010) 121.
34. Y. C. Lu, D. G. Kwabi, K. P. C. Yao, J. R. Harding, J. Zhou, L. Zuin, and Y. Shao-Horn, *Energy and Environmental Science*, **4**, 2999 (2011).
35. X. L. Li and A. Faghri, *Energy*, **36** 403 (2011).

Downloaded on 2014-09-24 to IP **77.236.37.84** address. Redistribution subject to ECS terms of use (see **ecsdl.org/site/terms_use**) unless CC License in place (see abstract).